ARMY RESEARCH LABORATORY

Mechanical Testing of 3D Fabric Composites and Their Matrix Material SC-15

by Brian Justusson, Jian Yu, Albert Chen, and Chian-Fong Yen

ARL-TR-6245 **November 2012**

NOTICES

Disclaimers

The findings in this report are not to be construed as an official Department of the Army position unless so designated by other authorized documents.

Citation of manufacturer's or trade names does not constitute an official endorsement or approval of the use thereof.

Destroy this report when it is no longer needed. Do not return it to the originator.

Army Research Laboratory
Aberdeen Proving Ground, MD 21005

ARL-TR-6245 **November 2012**

Mechanical Testing of 3D Fabric Composites and Their Matrix Material SC-15

Brian Justusson, Jian Yu, and Albert Chen
Oak Ridge Institute for Science and Education (ORISE)

Chian-Fong Yen
Weapons and Materials Research Directorate, ARL

REPORT DOCUMENTATION PAGE	Form Approved OMB No. 0704-0188

PLEASE DO NOT RETURN YOUR FORM TO THE ABOVE ADDRESS.

1. REPORT DATE *(DD-MM-YYYY)*	2. REPORT TYPE	3. DATES COVERED (From - To)
November 2012	Final	August 2012

4. TITLE AND SUBTITLE
Mechanical Testing of 3D Fabric Composites and Their Matrix Material SC-15

5a. CONTRACT NUMBER

5b. GRANT NUMBER

5c. PROGRAM ELEMENT NUMBER

6. AUTHOR(S)
Brian Justusson*, Jian Yu*, Albert Chen*, and Chian-Fong Yen

5d. PROJECT NUMBER
H84

5e. TASK NUMBER

5f. WORK UNIT NUMBER

7. PERFORMING ORGANIZATION NAME(S) AND ADDRESS(ES)
U.S. Army Research Laboratory
ATTN RDRL-WMM-B
Aberdeen Proving Ground, MD 21005

8. PERFORMING ORGANIZATION REPORT NUMBER
ARL-TR-6245

9. SPONSORING/MONITORING AGENCY NAME(S) AND ADDRESS(ES)

10. SPONSOR/MONITOR'S ACRONYM(S)

11. SPONSOR/MONITOR'S REPORT NUMBER(S)

12. DISTRIBUTION/AVAILABILITY STATEMENT
Approved for public release; distribution unlimited.

13. SUPPLEMENTARY NOTES
*Oak Ridge Institute for Science and Education (ORISE)

14. ABSTRACT

The U.S. Army is actively investigating advanced light-weight structural materials for protective applications in combat vehicles. One such class of materials is Fiber Reinforced Polymer Composites (FRPC). FRPC are a class of materials that consist of a polymeric matrix that is reinforced through the inclusion of long fibers that are bundled together in a structure known as a fiber tow. Traditional FRPC structures generally contain stacks of individual layered fabrics (lamina) oriented in a particular fiber orientations. This traditional FRPC has anisotropic architectures that lead to the development of large interlaminar shear stresses between adjacent layers. The built up of shear stress would ultimately delaminate the composite. To counter the delamination failure, a new class of FRPC has been developed by weaving fiber tows together. The weaving technique eliminates or reduces much of the shear stresses accumulation between the adjacent layers at large angles. Despite this, delamination may still occur. In an effort to further reduce the delamination mode of failure, researchers have proposed the addition of through the thickness reinforcement. The proposed methods such as z-pinning and stitching; however, can often damage fiber tows and result in large losses in plane stiffness. Another through the thickness method is 3D weaving. It involves the use of an additional yarn, which integrally binds the fabric layers together. The addition of the through thickness yarn can suppress and even eliminate the delamination mode of failure altogether. While much is known about the mechanical performance of woven composites, little has been done to understand how the 3D weaving architecture affects the mechanical performance. The effect of architectural weaves on the progression of failure in both quasi-static tension and compression are examined.

15. SUBJECT TERMS
3D fabric composite SC-15 compression tensil mechanical properties

16. SECURITY CLASSIFICATION OF:			17. LIMITATION OF ABSTRACT	18. NUMBER OF PAGES	19a. NAME OF RESPONSIBLE PERSON
a. REPORT	b. ABSTRACT	c. THIS PAGE			Jian Yu
UNCLASSIFIED	UNCLASSIFIED	UNCLASSIFIED	UU	32	19b. TELEPHONE NUMBER (*Include area code*) 410-306-0698

Standard Form 298 (Rev. 8/98)
Prescribed by ANSI Std. Z39.18

Contents

List of Figures iv

List of Tables iv

1. Introduction/Background 1

2. Experiment and Calculations 2

2.1 Sample Fabrication 2

2.2 Tensile Tests for Matrix 3

2.3 Compressive Tests for Matrix 4

2.4 Tensile Tests for Composites 5

2.5 Compression Tests for Composites 6

3. Results and Discussion 6

3.1 Mechanical Properties of the Matrix 6

3.1.1 Tensile Response of the Matrix 7

3.1.2 Compressive Response of the Matrix 8

3.2 Mechanical Properties of the Composite 9

3.2.1 Tensile Response of the Composite 10

3.2.2 Compressive Response of the Composite 17

4. Summary and Conclusions 20

5. References 22

List of Symbols, Abbreviations, and Acronyms 24

Distribution List 25

List of Figures

Figure 1. The cure cycle used for the for the SC-15 epoxy for mechanical characterization. 3
Figure 2. Schematic showing how the 6 different strain measures were taken in the SC-15 samples. 4
Figure 3. Side image showing the applied speckle and cropped raw image for compressive tests of the SC-15. 4
Figure 4. Sample dimensions for a modified dogbone sample. 5
Figure 5. The global stress-strain behavior of SC-15 in both tension and compression. 7
Figure 6. The stress strain response of the SC-15 for (a) the current work and (b) against previous reported data. 8
Figure 7. Results of compression testing of the SC-15 matrix material. 9
Figure 8. The results of tensile testing for the S2 glass orthogonal weave. 11
Figure 9. The results of tensile testing for the Carbon/S2 glass hybrid orthogonal weave. 12
Figure 10. Schematic showing how matrix cracks develop from weaving pockets and lead to progressive failure. 12
Figure 11. Progressive failure analysis of the S2 glass samples in the warp and weft direction under tension. 13
Figure 12. Photographs of sample failures in tension for S2 glass samples. 14
Figure 13. Photographs of sample failures in tension for Carbon/S2 glass samples. 15
Figure 14. Progressive failure analysis in the carbon/S2 hybrid samples in warp and weft direction under tension. 16
Figure 15. The results of compressive testing for the S2 glass orthogonal weave. 17
Figure 16. The results of compressive testing for the Carbon/S2 glass hybrid orthogonal. 18
Figure 17. Photographs of sample failures in compression for S2 glass samples. 19
Figure 18. Photographs of sample failures in compression for the Carbon/S2 glass sample. 19
Figure 19. Photographs of the failure surfaces for each of the tested surfaces showing that the architecture may affect mechanical performance. 20

List of Tables

Table 1. Results of the mechanical testing for SC-15 matrix material. 7
Table 2. Results of current SC-15 against previously published data. 9
Table 3. Global results of mechanical testing of composite materials. 10

1. Introduction/Background

Fiber Reinforced Polymer Composite (FRPC) materials are desirable structural materials for military applications because they offer a high stiffness to weight ratio. The implementation of these structural materials on military vehicles allows increased agility while maintaining a light-weight primary structure. Traditional laminated structures suffer from delamination under a variety of loading conditions. One such loading condition that is critical for composite application on military vehicles is impact loading. Olsson showed that delamination as a result of impact degrades both stiffness and strength (*1*). As Olsson suggests, the delamination mode is particularly serious because it forms at low loads and greatly affects mechanical performance.

In order to combat the delamination mode of failure, three techniques have been proposed: the use of Z-pins, stitching, and 3D weaving. Each of these techniques has performed sufficiently well in reducing or eliminating delamination all together. Z-pinning is the mechanical insertion of through thickness reinforcement by using stiffened pins into the plies. Huang and Waas have shown experimentally (*2*) and computationally (*3*) that the insertion of even 1% of Z-pins reduces the strength. Mouritz and Cox showed that damage can be induced through Z-pin insertion, but also results in the creation of resin rich areas that can aid in premature failure (*4*); however, improvements in reduction of delamination are apparent.

Through thickness stitching is the binding of layers together by the use of an additional fiber yarn that is mechanically stitched into the preform. The effects of stitching are a little less certain. Mouritz and Cox have shown in their review that stitching can retain or even improve mechanical performance where the reduction in mechanical performance is attributed to the damaging of the fibers during stitching (*4*). The resistance to impact with stitched composites was reviewed by Dransfield (*5*) and studied by Tan for compression after impact strength. Tan found that the higher stitch densities result in improved compressive behavior after impact as a result of localization of damage (*6*).

3D Woven Composite (3DWC) is a new class of composite material that relies heavily on the woven based design to achieve a desired mechanical performance. The woven architecture design incorporates a series of rigid warp and weft yarns whose layers are bound together with an additional through the thickness reinforcement or binder yarn during the weaving process of the 3DWC. There are several different types of 3DWC architectures, which include orthogonal, angle-interlock, layer-to-layer, braiding, and knitting. The weaving process, however, can damage the fibers prior to curing with the resin (*7*). This in turn results in decreased mechanical performance as damaged fibers provide a path for cracks to propagate (*8*).

Failure of 3DWC under quasi-static loading has been investigated in great detail. Cox et al. studied the failure mechanics of 3DWC in tension (*9*), compression, and bending. They found that a variety of failure mechanisms are working all at once, but each is dependent on the compaction and thusly architecture of the sample (*10*). Quinn et al. noted that crimping of the binder tows reduces the efficiency of the structure and that large binding yarns create resin rich areas (*11*).

While these initial observations offer a qualitative look into the failure mechanics of 3DWC, more experimental information is needed. Full-field strain measurements lend insight into how the architecture affects the mechanical performance due to the creation of matrix pockets. Measurements can be made using shearography (*12*), Moiré interferometry fringe patterns (*13*) or Digital Image Correlation (DIC) (*14*). This type of information is vital to accurately understand how the woven architecture affects the mechanical performance.

In this report, detailed experimental work was conducted to provide novel insight to the progression of failure in two 3D textile composite systems. Included in this study is an evaluation of the matrix material, SC-15. The matrix material properties have been widely reported in a number of different research groups; however, there is no clear consensus among researchers. The matrix material is tested to the American Society for Testing and Materials (ASTM) standards for polymeric materials and failure modes in both tension and compression are examined. The first 3D textile is a 3/8-inch (in) equivalent S2 glass fiber orthogonal weave. In this weave, a single z-yarn at approximately 6% is used to integrally bind the layers together. The second 3D textile is a hybrid IM7 carbon fiber and with two S2 glass z-yarns. The S2 is again approximately 6%. Both types of textiles were subjected to tension and compression. A progression of failure will be presented in this work along with examination of failure modes.

2. Experiment and Calculations

2.1 Sample Fabrication

Two fabric pre-forms were woven by two different textiles manufacturers. An equivalent 3/8-in all S2 glass fabric was woven by Textiles Engineering and Manufacturing (TEAM) and consisted of a single z-yarn through the thickness. A hybrid fabric pre-form was woven by 3Tex and featured two z-yarns made of carbon fibers in the warp and weft directions. The pre-forms were infused using a Vacuum Assisted Resin Transfer Molding process with SC-15 epoxy resin system. From the bulk sample, tension and compression samples were extracted from the panels using a waterjet cutting system.

A second panel of pure SC-15 matrix was then made to analyze the response of the material in both tension and compression. The epoxy was given a typical cure cycle that is used for the composite materials and is shown in figure 1. The SC-15 matrix was cured into a

20-in × 20-in × 1/8-in panel. Tension and compressive samples were cut from the panel using water jet.

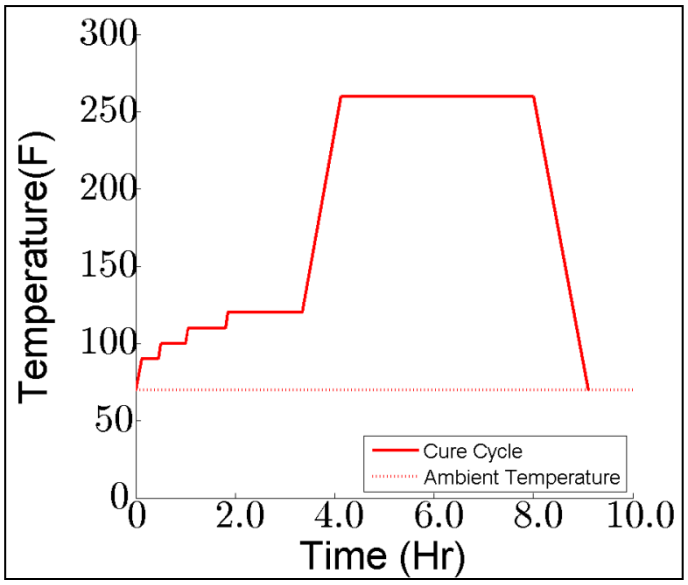

Figure 1. The cure cycle used for the for the SC-15 epoxy for mechanical characterization.

2.2 Tensile Tests for Matrix

Tensile tests were performed according to the ASTM D638 (*15*) specification; however, strain was measured optically instead of the use of a digital strain gauge. Photographs were taken by a CCD camera at a rate of 10 Hz. Load and displacement was also recorded by the DAQ at a rate of 10 Hz. The strain was measured using the commercial software ProAnalyst (*16*). From the analysis software, nine points were selected for analysis. A sample of how the points were selected is shown in figure 2. Three of these points were aligned on the tensile axis in the center of the specimen, and six were selected on the side of the sample. From the center axis, three strains were recorded and averaged to give the total strain in the sample in the longitudinal direction. Additionally, three strains were averaged to get the transverse strain. These measurements are equivalent to what would be measured by the strain gauge. However, since this technique is not limited to a single point, as strain gauges are, the strain measured actually covers a broader area of the specimen.

From the tensile tests, four major mechanical properties were determined: the modulus of elasticity, the ultimate tensile strength, the failure strain, and the Poisson's Ratio. The modulus of elasticity was determined by taking the slope of the linear portion of the response. The linear elastic portion of the curve was generally between 0.5% and 1.0% strain. The ultimate tensile strength was determined by the maximum stress experienced by the sample before failure. The failure strain was determined by the average longitudinal strain at failure. The Poisson's ratio

was determined by taking the slope of the longitudinal strain versus the transverse strain curve during the elastic loading.

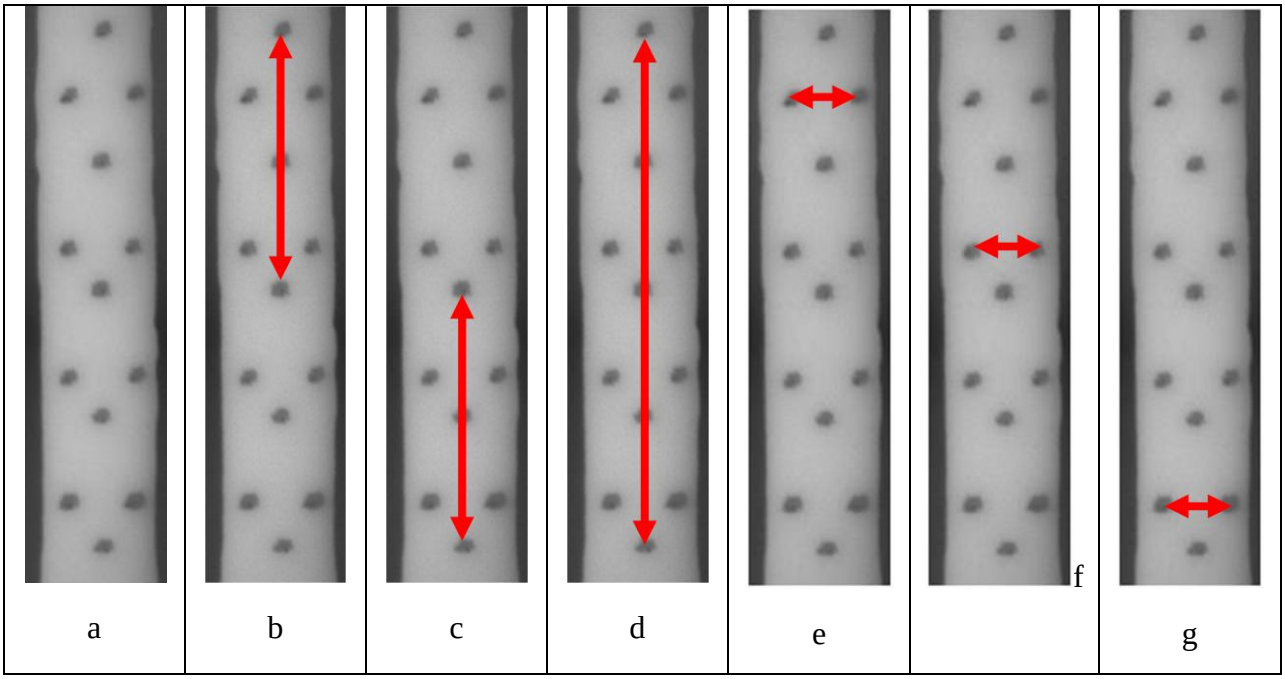

Figure 2. Schematic showing how the 6 different strain measures were taken in the SC-15 samples.

2.3 Compressive Tests for Matrix

Compression tests for the matrix were performed according to the ASTM D695 specification (*17*). The samples were loaded at a rate of 0.05 in/minute. Strain gauges were not used for this testing because strains beyond the failure strain of the gauges were expected. Instead, a speckle pattern was applied to the side of the sample using Krylon fusion paint. Images were then taken every two seconds using a Nikon D80 digital SLR camera. The images were then cropped using a MatLab script and were analyzed using the ARAMIS DIC software (*18*). A sample of the raw image is seen in figure 3.

Figure 3. Side image showing the applied speckle and cropped raw image for compressive tests of the SC-15.

ARAMIS DIC software then calculated the corresponding strain fields. This was used to generate a stress-strain response in compression. From this data, the failure strain, failure

strength, modulus of elasticity and Poisson's ratio were determined. The modulus of elasticity was determined by taking the slope of the linear elastic portion of the curve. This was done by taking the slope of strains from 0.1%–1.5%. The failure strength was determined from the maximum stress in the sample, and the failure strain was the strain at failure. The Poisson's ratio was determined by taking the slope of the transverse-longitudinal strain curve.

2.4 Tensile Tests for Composites

Traditional tensile tests for composites do not necessarily work well with 3D textile composites. This is because failure modes are often seen that do not correspond with the ASTM specification such as that of D639 and D3039 (*19*). For this reason, a modified dog-bone sample was used. Additionally, the fibers are too strong for specification D639 and tab failure is commonly seen using specification D3039. The dimensions of the sample are shown in figure 4. This geometry was selected because it has performed well in the past for obtaining tensile failure, but also has a large grip section that does not induce damage to the gage section during loading.

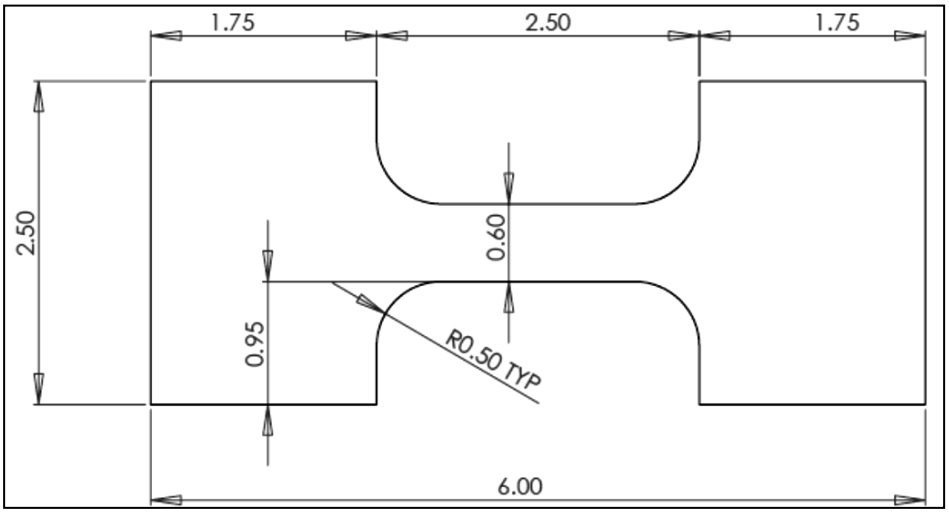

Figure 4. Sample dimensions for a modified dogbone sample.

A total of five samples were tested in both the warp and the weft direction. The samples were tested at a rate of 0.0004 inch/second (in/s) and a random speckle pattern was applied to the sample using Krylon fusion spray paint to create a contrast. Contrast was created by applying a white paint to the carbon surface and a black paint to the white glass surface. If necessary, additional speckles were added using silver or black Sharpies. Images were taken using a Nikon D80 at a rate of one image every 5 seconds (s). The load-time history was collected using a DAQ at a rate of 10 Hz. The stress was determined by dividing the load by the average of three cross-sectional area measurements. The strain-time history was determined using ARAMIS DIC software and the entire stress-strain behavior was determined by correlating the strain-time history and stress-time history through interpolation techniques in time.

The results were analyzed to determine the modulus of elasticity, failure strain, and ultimate tensile strength. The modulus of elasticity was determined by using a linear fit to the data between the strain ranges of 0.25%–1.25%. This was selected because at 0.25% strain most of the compliance or bending in the sample has been eliminated. The failure strain was determined by finding the maximum strain at failure, and the ultimate tensile strength was determined from the maximum stress the sample experienced.

Since the DIC strain measurements were performed on an in plane surface relative to the fiber direction, the Poisson's ratio in the 1–2 direction, v_{12} could be determined by plotting the resulting strain in the orthogonal direction. The Poisson's ratio is reported so that the loading direction refers to the first index. For example, if loaded in the warp direction, the 1 corresponds to the warp direction, and the 2 corresponds to the weft direction. To calculate the ratio, the slope of the plot was taken from the $\varepsilon_1$versus ε_2 using a linear fit. Points from the initial loading and near failure were neglected as they did not give an accurate representation of the ratio.

2.5 Compression Tests for Composites

Compression tests were performed in accordance with the ASTM D6641 (Standard Test Method for Compressive Properties of Polymer Matrix Composite Materials Using a Combined Loading Compression [CLC] test fixtures) test procedure (*20*). Samples were cut to 5.5 in × 0.5 in. The thickness of the S2 glass varied considerably on the bag side; therefore, the bag surface was ground down to allow for proper combined loading the samples.

The sample was loaded at a rate of 0.05 inch per minute (in/min). Due to the relative short duration of the test, images were taken with a Nikon D80 at a rate of one picture per 2 s. The load-time history was collected using a DAQ at a rate of 10 Hz. The stress in the sample was determined by dividing the load by the average of three cross-sectional area measures. The strain-time history was again determined with the ARAMIS DIC software. To determine the mechanical properties, the sample procedure was used as described in the tensile section.

DIC strain measurements were performed on a through thickness plane relative to the fiber direction, the Poisson's ratio in the 1–3 direction, v_{13} could be determined by plotting the resulting strain in the orthogonal directions. The procedure for determining the ratio was the same as described in the tensile tests.

3. Results and Discussion

3.1 Mechanical Properties of the Matrix

The mechanical properties of the matrix are shown in table 1. Included in the results are the modulus of elasticity, failure strength, Poisson's ratio and failure strain. Of particular interest is the fact that there was a different mechanical response depending on the type of loading. In

compression, the SC-15 showed by a higher modulus of elasticity and a higher failure strain. This is an interesting result because the material is generally believed to be isotropic. From the two tests, the Poisson's ratio was found to be approximately 0.40 in both tension and compression; however, there is a higher level of confidence in compression. The compressive sample showed higher strains to failure, though this may not be a true measure of the failure strain. As the material strains further, a shearing instability develops that allows the loading head to come in contact with the support jig. This results in higher loads as the material is no longer the sole load carrying structure in the test. For this reason, the failure strain is reported as the strain where the instability begins.

The complete stress-strain behavior of the material is shown in figure 5, which includes both the tensile and compressive mechanical response. This figure illustrates the fact that there is a different response depending on the loading direction. For this reason, it is important to develop a material model that accounts for both the tensile and compressive response.

Table 1. Results of the mechanical testing for SC-15 matrix material.

Sample	Test Direction	Modulus of Elasticity (GPa)	Failure Strength (MPa)	Poisson's Ratio (v)	Failure Strain (%)
SC-15 Matrix Material	Tension	2.20 ± 0.18	58.31 ± 2.24	0.36 ± 0.08	4.23 ± 0.48
	Compression	2.51 ± 0.03	76.95 ± 1.01	0.40 ± 0.07	4.84 ± 0.69

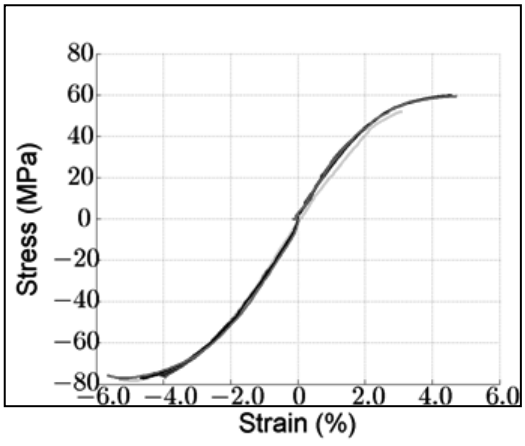

Figure 5. The global stress-strain behavior of SC-15 in both tension and compression.

3.1.1 Tensile Response of the Matrix

The stress strain mechanical response of SC-15 in tension is shown in figure 6. The eight samples that were tested until failure are shown in figure 6a. Of particular interest, the results are fairly consistent in modulus of elasticity and ultimate tensile strength. The modulus was

determined to be 2.20 ± 0.18 GPa and the UTS was 58.31 ± 2.24 MPa. The sample generally showed a bilinear response with some pronounced plasticity effects. Necking however, was not observed. The samples generally failed at strains of less than 5%, which demonstrates there is not a particularly high amount of ductility. This however, was to be expected as SC-15 is a thermoset plastic. This type of behavior is similar to other matrix materials.

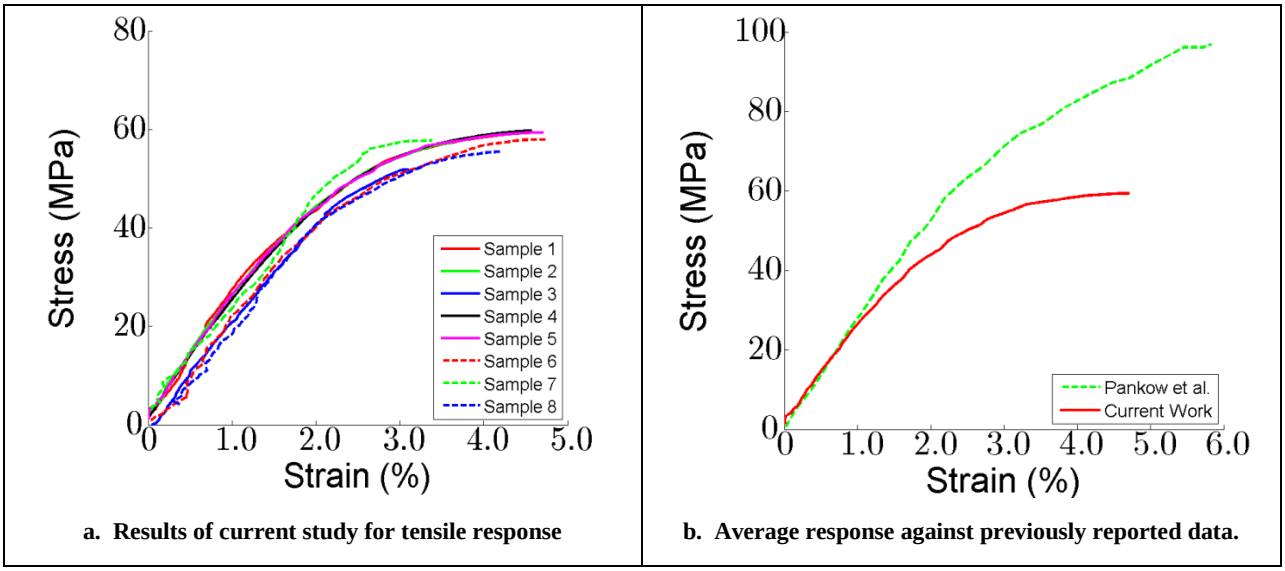

a. Results of current study for tensile response

b. Average response against previously reported data.

Figure 6. The stress strain response of the SC-15 for (a) the current work and (b) against previous reported data.

3.1.2 Compressive Response of the Matrix

The results of the compression testing for all 5 samples are shown in figure 7. From figure 7, it is clear that each of the tests is nearly identical in terms of mechanical performance. The failure strengths and modulus are very similar which results in little error in reporting the mechanical properties. The largest amount of variation is in the failure strain. This problem was discussed earlier and may not in fact be the failure strain in compression. Further characterization would be needed, however, for the SC-15 currently used, the ASTM D695 does not allow for sufficient strains to cause failure.

The results of both the current effort and the results of previously published values for SC-15 are shown in table 2. The work of Pankow (*21*) was completed using a torsion test and tensile properties were extracted. Additionally, two tests were conducted on SC-15 by Zhou in both flexural testing (*22*) and tension testing (*23*). The current modulus of elasticity as determined by the compression test is nearly identical to that of Pankow; however the Poisson's ratio is not the equivalent. The failure strain is perhaps the most interesting of the mechanical data. Both Pankow and Zhou report a failure strain above 6.0%; however, in neither compression nor tension in the current effort is able to achieve strains as high as 6.4%.

The failure strains in the current work are similar with what was found previous with the work of Zhou (2007) but not with the work of Zhou (2005). Additionally, Zhou reports two failure

strengths that differ by as much as 50%. This could be attributed to two possibilities. First, this may be an artifact of the testing. In the work of 2005 (*22*), the stress-strain behavior was determined by the use of a flexural test, whereas the 2007 (*23*) work was determined by a tensile test. In general, the tensile test mechanical properties are similar to those of the current work. It is possible that deviations in the test setup could lead to improper interpretations of the results. Secondly, the author does not report a curing cycle. The curing cycle has a significant effect on the amount of cross-linking that occurs in the polymer and could ultimately be responsible for differences in mechanical performance.

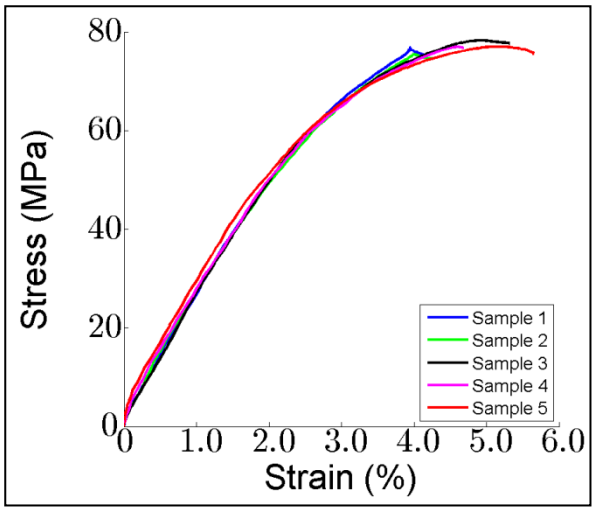

Figure 7. Results of compression testing of the SC-15 matrix material.

Table 2. Results of current SC-15 against previously published data.

Test Reporter	Modulus of Elasticity (GPa)	Failure Strength (MPa)	Poisson's Ratio (ν)	Failure Strain (%)
Pankow et al. (*21*)	2.487	110	0.35	6.4
Zhou et al. (2005) (*22*)	2.25 ± 0.11	85.0 ± 4.3	n/a	6.0
Zhou et al. (2007) (*23*)	2.31 ± 0.12	53.01 ± 2.79	n/a	4.86 ± 0.34

3.2 Mechanical Properties of the Composite

The results of the mechanical testing of the two types of composites are shown in table 3. There are a few points of interest that are worth further evaluation and will be discussed in greater detail in the subsequent sections. The first observation is that there always appears to be one direction that exhibits a higher modulus and failure strength than the other in the case of the S2-glass/Carbon hybrid panel. This would suggest that there is a higher yarn percentage in the warp direction than the weft direction.

The S2 sample, on the other hand, shows that there is much better balance of yarn fractions in the composite. In tension and compression, the weft direction is stiffer than the warp direction. The failure strengths are nearly identical in the warp and weft direction for both tension and

compression. The warp direction displays higher strains to failure both in compression and tension. Of particular note, the Poison's ratio, v_{12}, was found to be minimal in the warp direction. This may be a result of the selected architecture having a weft yarn on the outer surface of the composite. In this regard, when the material is strained, there is a strong resistance to the Poisson's effect provided by the relatively stiff fibers.

Table 3. Global results of mechanical testing of composite materials.

Sample	Textile Direction	Test Method	Modulus of Elasticity (GPa)	Failure Strength (MPa)	Failure Strain (%)	Poisson's Ratio (v)
3/8-in S2 Glass Orthogonal Weave	Warp	Tension	18.2 ± 1.7	551.2 ± 65.7	3.16 ± 0.15	0.02 ± 0.01*[1]
		Compression	24.1 ± 3.4	330.7 ± 43.6	1.17 ± 0.29	0.58 ± 0.20[2]
	Weft	Tension	22.0 ± 0.7	521.3 ± 44.8	2.27 ± 0.18	0.13 ± 0.04[3]
		Compression	25.2 ± 3.4	333.9 ± 10.2	0.99 ± 0.31	0.73 ± 0.17[4]
¼-in Carbon/S2 Glass Hybrid Orthogonal Weave	Warp	Tension	80.1 ± 1.3	735.9 ± 51.7	1.00 ± 0.09	0.11 ± 0.02[1]
		Compression	59.7 ± 11.8	395.2 ± 7.9	0.47 ± 0.13	0.57 ± 0.18[2]
	Weft	Tension	68.5 ± 4.5	544 ± 12.1	0.79 ± 0.03	0.15 ± 0.01[3]
		Compression	39.6 ± 6.0	273.4 ± 2.8	0.58 ± 0.12	0.76 ± 0.04[4]
	**Poisson's Ratio effectively found to be 0* [1] v_{12}, [2] v_{13}, [3] v_{21}, [4] v_{23}					

The Carbon/S2 glass samples show a much different behavior than that of the S2 only samples. The first is that the material does not have the same yarn balance as the first material system. This is best shown by the fact that the material has a higher modulus in both tension and compression in the warp and the weft direction. Additionally, there are higher values of the ultimate tensile strength. There is a lower failure strain reported in the weft direction. There is a much different response in the compressive mode than that characterized by a lower failure strains and strengths.

3.2.1 Tensile Response of the Composite

The results of testing for four specimens in each direction are shown in figure 8 for both the warp (a) and weft directions (b). From these plots, it is clear that the modulus of elasticity and failure strain behavior are very similar for this composite in these two directions. The weft direction displays a higher degree of repeatability and is most likely due to the fact that the weft

yarns are held straight during the weaving process. These weft yarns therefore have fewer local undulations and thusly, have minimal load transfer along the fiber's length. On the average, the failure strengths and the modulus of elasticity were higher in the weft direction, but were in agreement within the measured error.

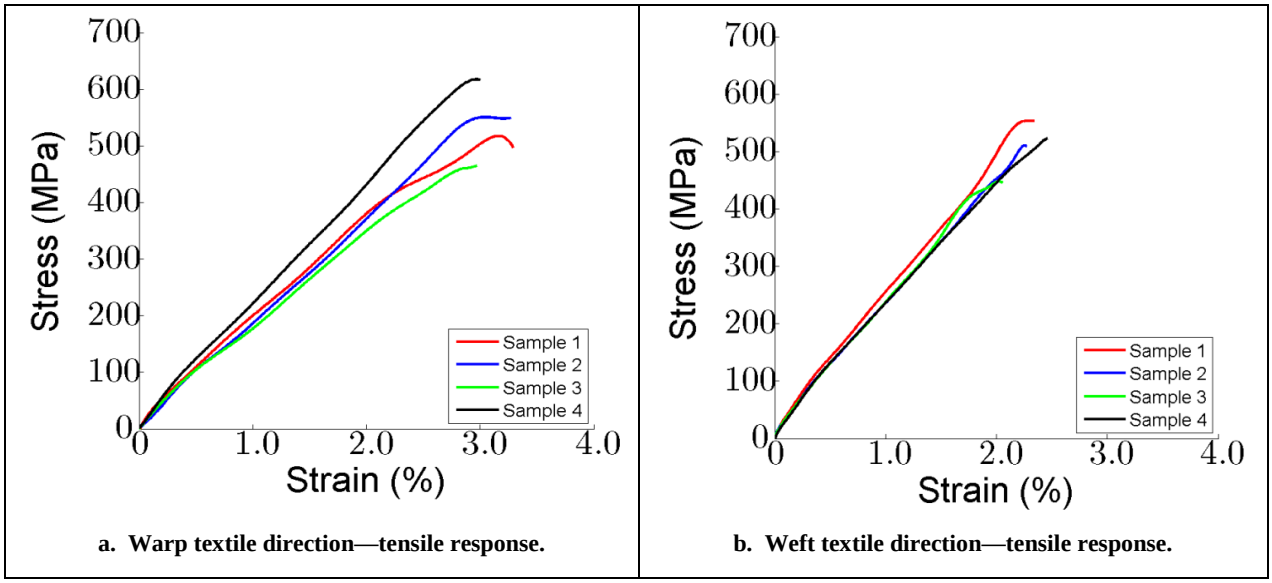

a. Warp textile direction—tensile response.

b. Weft textile direction—tensile response.

Figure 8. The results of tensile testing for the S2 glass orthogonal weave.

The tensile samples for the carbon/S2 glass showed interesting behavior. The warp direction was significantly stronger than the weft direction as shown in figure 9. This is most likely due to the fact that there are a larger percentage of fibers in the warp direction. This also can explain the higher stiffness. In general, the samples showed a linear elastic behavior with no apparent damage effects. This would indicate that failure was catastrophic and rapid rather than a slow progression from the slow loading. In addition to higher strengths, the warp direction also had a behavior that shown higher failure strains and a higher modulus of elasticity.

When examining the failure behavior of the samples, it is clear that the samples did not fail in the gauge section; however, this is not an uncommon failure for 3D textiles. Because the samples are very stiff in both orthogonal directions, it is not uncommon to have a failure mode of fiber tow/matrix debonding. This is due to the fact that the fiber tows are quite strong; however, there is an influence of the architecture on this type of failure. As the strain develops in the material, there is preferential matrix cracking that begins. The matrix cracks occur because there is a high concentration of stress that develops at matrix pockets that are a result of weaving. Callus et al. have shown that the weaving process creates resin channels that allow cracks to form for glass fiber reinforced polymers (*24*). As the accumulated strain in the sample increases, the cracks grow. This then allows for cracking around the tows to occur and subsequent debonding of the fiber tows with the matrix material. This type of failure is similar to that reported in Cox et al. as

an energy dissipation mechanism that allows for higher loads to be carried by the fiber tow prior to rupture (*10*). A schematic of this effect is shown in figure 10.

Figure 11 shows the evolving surface strains for the S2 glass samples. As the samples begin to strain, the cracks develop as shown schematically in figure 10. These surface strains further allow for analysis to take place and provides valuable information for how the strain develops through the sample as a result of the architectures. From this, it is clear that the location of the z-yarn has where it binds the layers together allows for matrix cracking to occur.

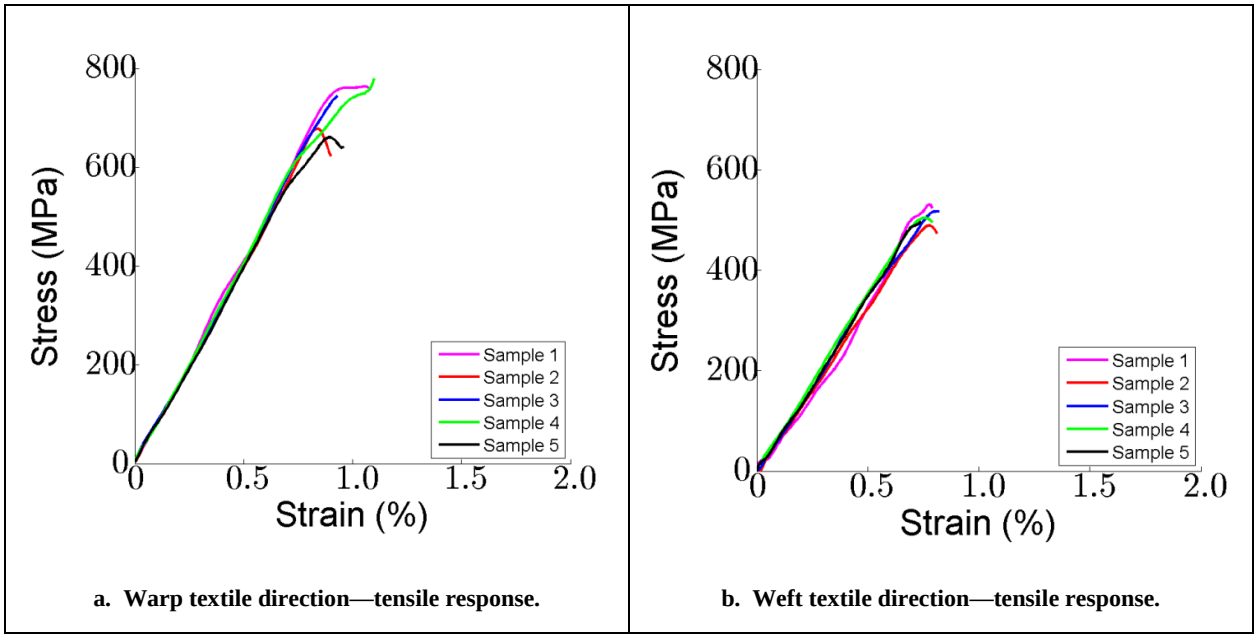

a. Warp textile direction—tensile response.

b. Weft textile direction—tensile response.

Figure 9. The results of tensile testing for the Carbon/S2 glass hybrid orthogonal weave.

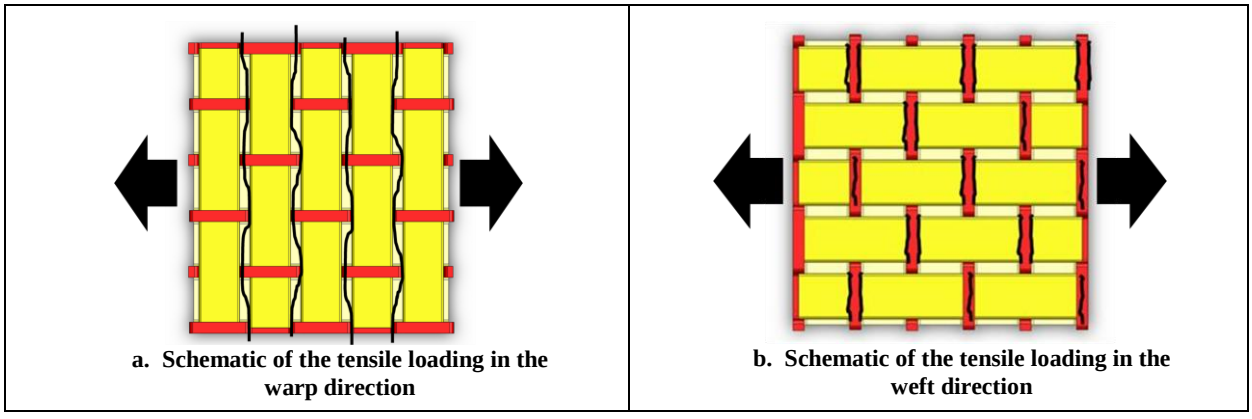

a. Schematic of the tensile loading in the warp direction

b. Schematic of the tensile loading in the weft direction

Figure 10. Schematic showing how matrix cracks develop from weaving pockets and lead to progressive failure.

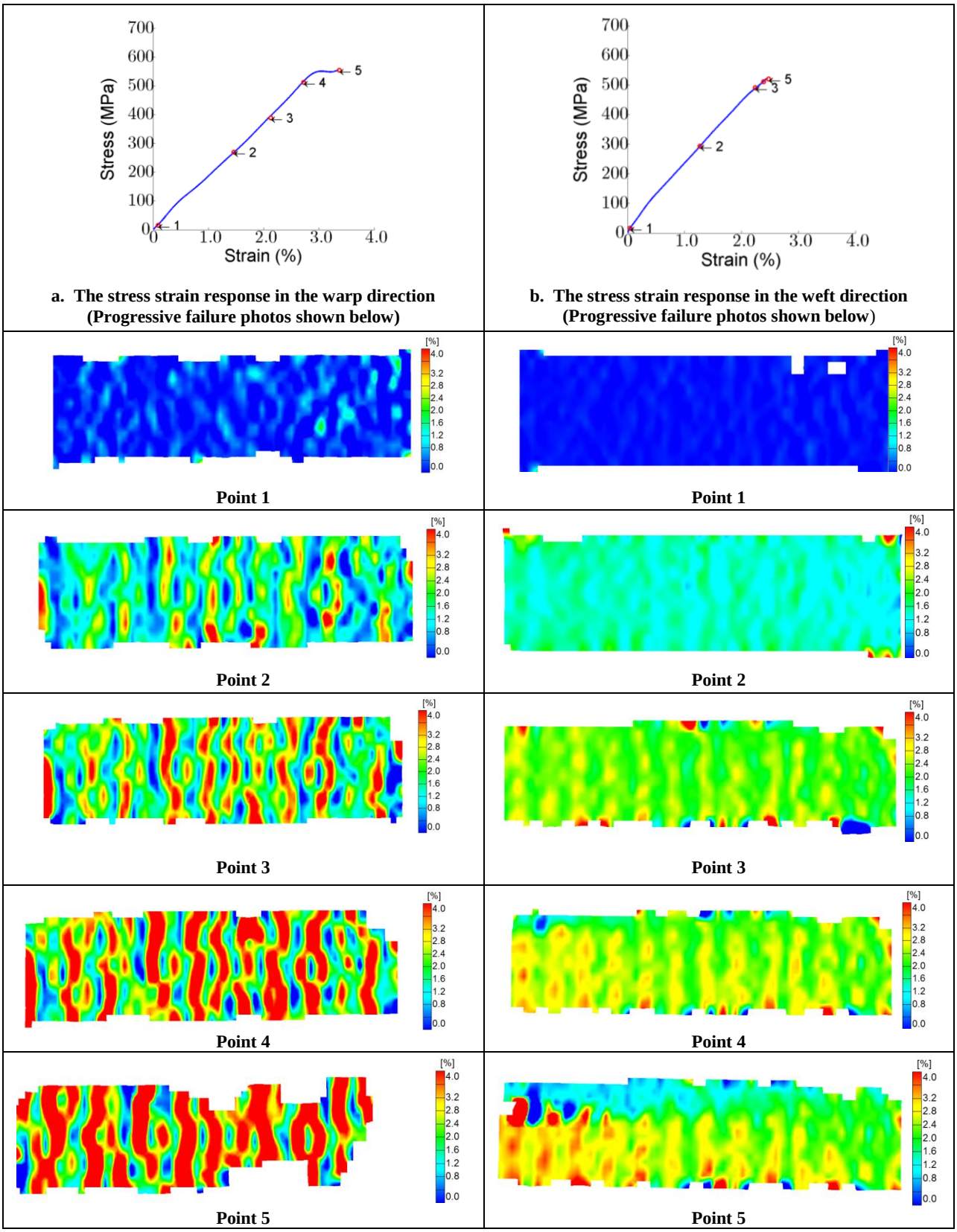

Figure 11. Progressive failure analysis of the S2 glass samples in the warp and weft direction under tension.

Figure 10 shows how two crack paths can develop, in the warp direction (a) and in the weft direction (b). Both of these failure modes develop as a result of the weaving pockets that are formed as a result of the weaving and subsequent VARTM process. The progression of the cracks is much different depending on the loading direction. Starting with the warp direction, the cracks begin to develop in the matrix pockets. As the cracks nucleate at different matrix pockets in the material, they begin to advance and coalesce. At a critical strain, the material is completely traversed by the crack and debonding between the matrix and fiber tows is observed. This then allows for failure to occur as the fibers then pull out of the matrix. The failure occurs at the radius of the dog-bone specimen due to the stress concentration. The stress concentration allows for higher stresses in the matrix material to occur and thusly higher strains at the matrix pockets. For this reason, the through the width matrix crack develops more rapidly. While load can still be sustained at this point, it is significantly less than the peak. This failure type is shown in figure 12a.

The cracking that develops in the weft direction shows a slightly different behavior for the weft samples. As the matrix cracks form, and begins to nucleate, they are suppressed by the addition of the weft fibers. Since the weft fiber is now closer to the surface than a preferential crack path from a matrix pocket, the crack is arrested when encountering the weft fiber. In this regard, there is no clear through the gauge section crack that forms. In this case, the failure is much more catastrophic. Debonding does occur, but, there is a higher failure strength that is observed because it is closer to a pure tensile failure. In this case, the cracks that develop are longitudinal relative to the loading direction. The failure in the weft direction is seen in figure 12b.

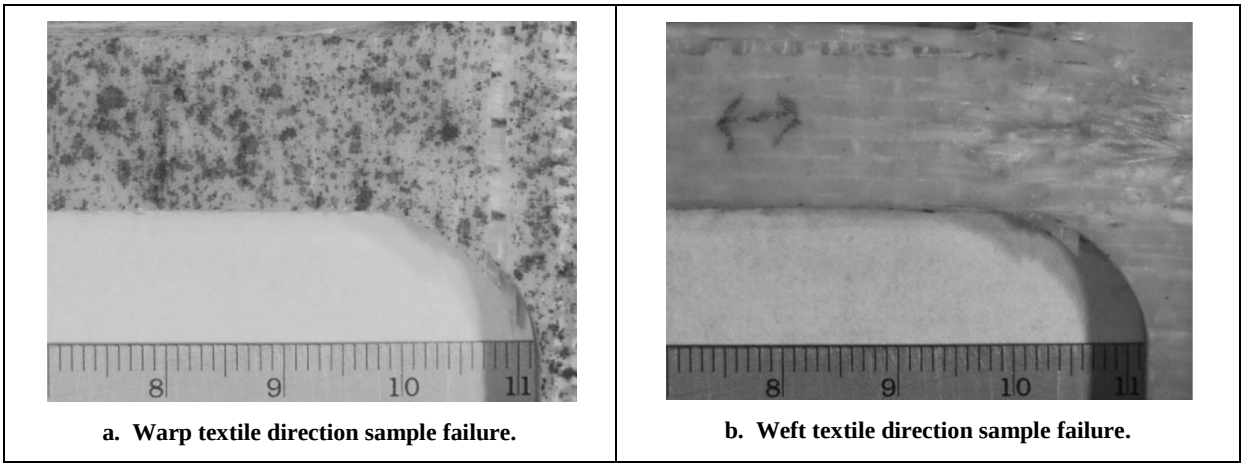

a. Warp textile direction sample failure.

b. Weft textile direction sample failure.

Figure 12. Photographs of sample failures in tension for S2 glass samples.

This same type of failure behavior was observed in the Carbon/S2 hybrid samples. As the material is strained, the same matrix cracks are beginning to form. These matrix cracks can be seen in the failure of the samples shown in figure 13. In the warp direction, shown in figure 13a, the cracks develop in the transverse direction; however, they do not propagate in a straight path. Since there is not a preferential path for the crack to follow, they must link together over long

distances. This accounts for the failure that is seen in the sample near the curvature. The failure is very similar to that of the pure S2 glass sample. By comparison, in the weft direction, shown in figure 13b, the sample shows a cracking pattern it is consistent with the S2 samples. In particular, there is a clear cracking that forms above and below the yarn in the transverse direction. The cracks however, do not propagate in the transverse direction, but rather in the longitudinal direction. The failure, therefore, is not the same as the warp direction, but rather the failure occurs on a random path that is architecturally related.

Figure 14 shows the progression of failure in the carbon/S2 glass samples which shows a similar behavior to that of the all S2 glass samples. Of particular importance is the periodicity of the strain fields. This indicates that there is not a clear crack path for the matrix cracks to follow and thusly, might be considered a better weaving architecture than the S2 samples.

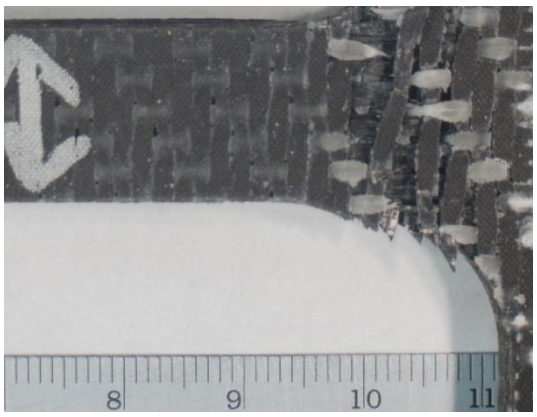

a. Warp textile direction sample failure.

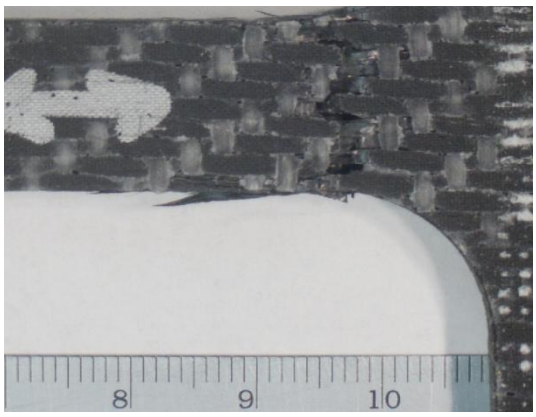

b. Weft textile direction sample failure.

Figure 13. Photographs of sample failures in tension for Carbon/S2 glass samples.

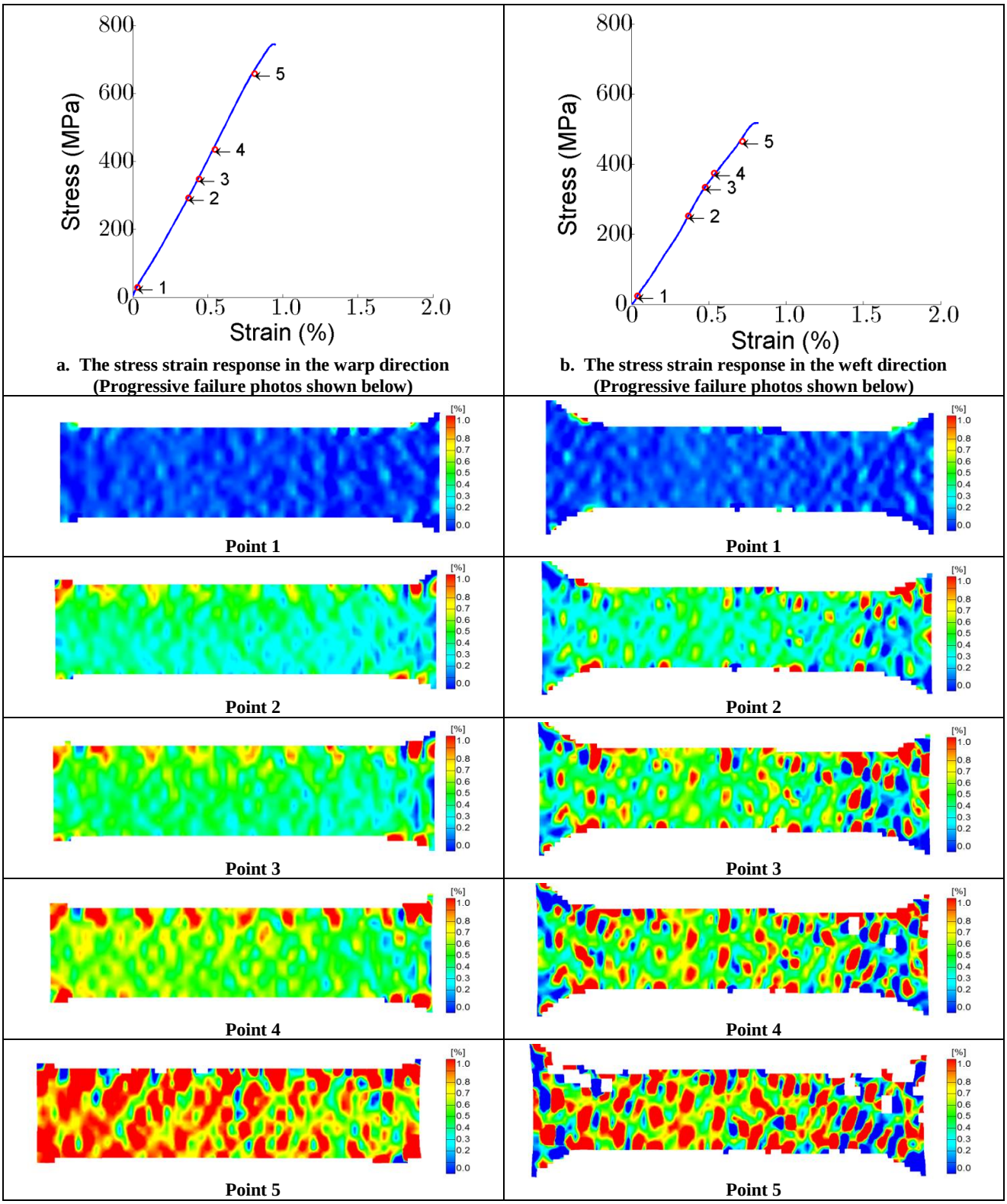

Figure 14. Progressive failure analysis in the carbon/S2 hybrid samples in warp and weft direction under tension.

3.2.2 Compressive Response of the Composite

Similar to the tensile samples, the S2 glass showed a characteristic agreement in mechanical performance. The samples in the warp direction showed that the modulus of elasticity and failure strengths are nearly identical. This is characteristic of a yarn fiber volume fraction being very similar. On the average, the weft direction showed higher failure loads and ultimate tensile strengths. One particular area of interest is that the specimen has a higher modulus of elasticity in compression than in tension. While this ordinarily would not be the case for an isotropic material, this could be a result of the matrix material performing better in compression. This could explain the apparent additional increase in strength. Similar behavior was observed in carbon/S2 glass hybrid. The results for the compressive testing of the S2 glass are shown in figure 15.

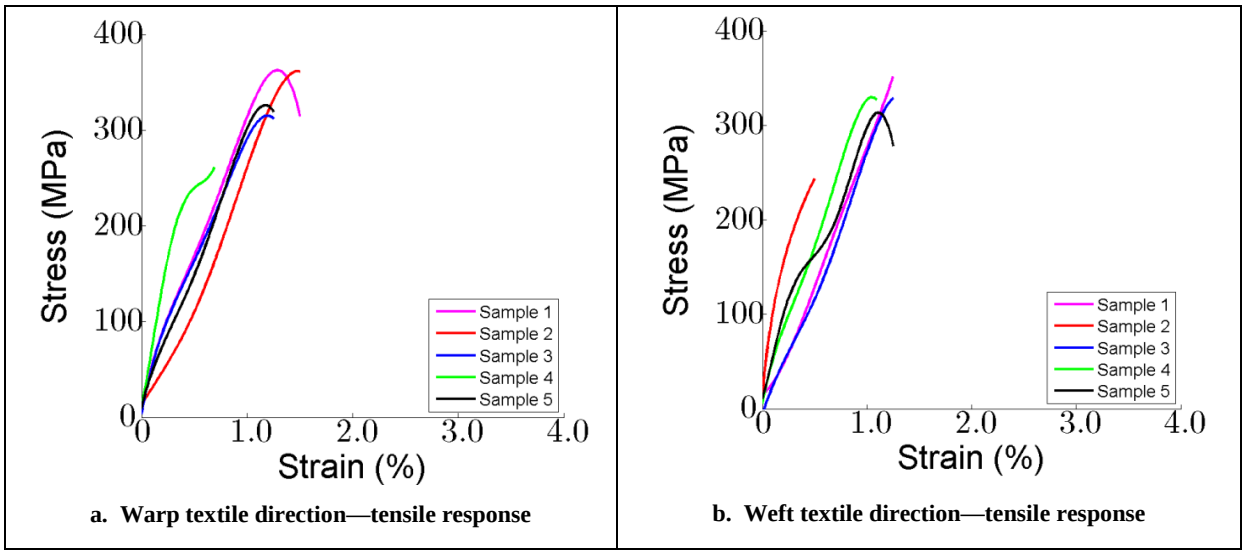

Figure 15. The results of compressive testing for the S2 glass orthogonal weave.

Figure 16 shows the results of the mechanical testing of the carbon/S2 glass hybrid sample in the warp (a) and weft (b) directions. As in the case of the tension, the warp direction shows much higher stiffness and failure strength. In the warp direction, there is some consistency between the tests. However, it is difficult to fully analyze the behavior due to the progression of failure. As the sample strained, a single failure mechanism was not observed in the weft direction, but rather a progression of failure that led to the ultimate "brooming" type failure in the samples.

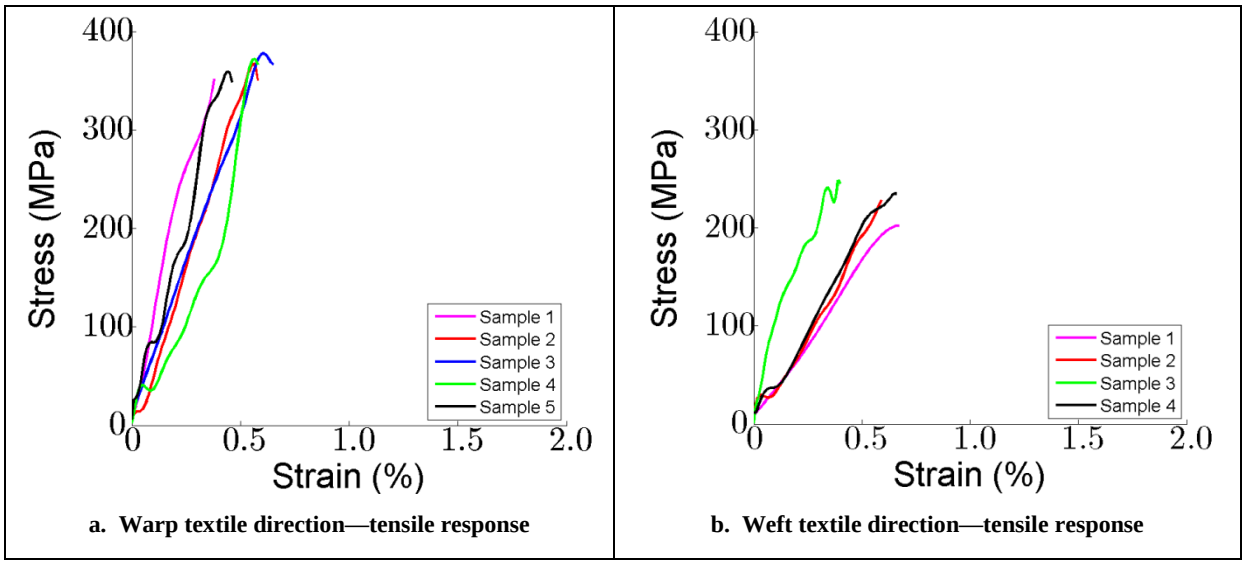

Figure 16. The results of compressive testing for the Carbon/S2 glass hybrid orthogonal.

The failure mechanism between the warp and the weft direction of the S2 glass sample was generally the same in each direction. Both of the samples failed through shear/kink band formation as shown in figure 17. After failure, no additional significant load carrying capability was preserved. The kink occurred in the gauge section of the sample, and formed very discretely as a single band through the material.

The failure mechanism for the carbon/S2 glass was much different. In the weft direction, shown in figure 18b, there is a failure surface that is similar to that of the S2 only glass samples. Instead of the formation of a single discrete band, multiple failure bands can be observed. This is most likely the result of the weaving pattern and the cracking that was discussed previously in tensile samples. The warp direction, shown in figure 18a, has an effect that is more similar to brooming than any other failure mode. As the sample continues to deflect, failure localizes and arrests itself in the material. This leads to several cracks developing through the material. The cracks might be arrested by the addition of the second z-fiber. This may result in a very interesting load dissipating ability of the material. This type of behavior was observed in all the samples in the warp direction and is consistent with the mini-band cracks that are described by Kuo et al. (*25*).

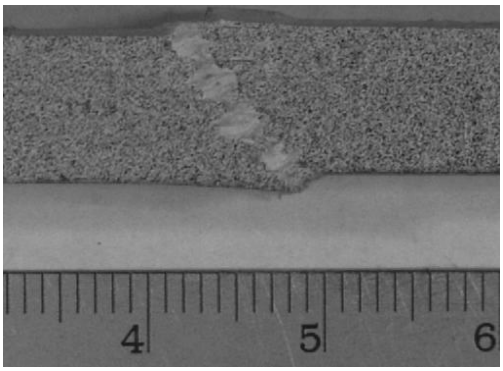

a. Warp textile direction sample failure.

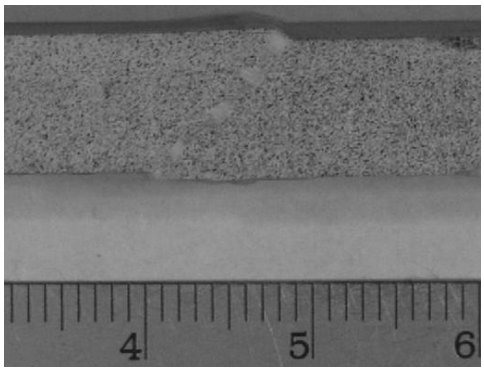

b. Warp textile direction sample failure.

Figure 17. Photographs of sample failures in compression for S2 glass samples.

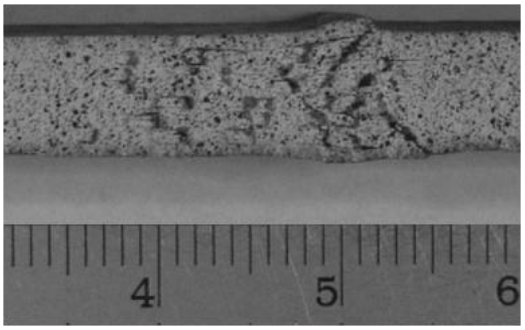

a. Warp textile direction sample failure.

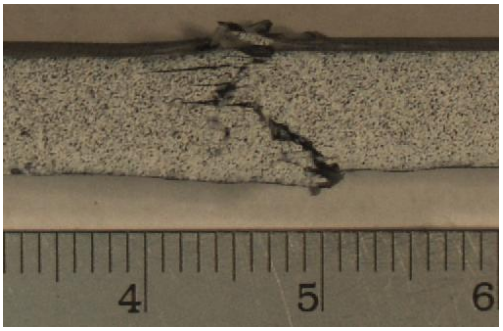

b. Weft textile direction sample failure.

Figure 18. Photographs of sample failures in compression for the Carbon/S2 glass sample.

Figure 19 shows the polished surfaces of the failed specimens shown in figure 17 and figure 18. From these images, it is clear that the failure in the warp direction (a) and weft direction (b) of the S2 glass composite is nearly identical in terms of failure type and mode. The failure for the carbon/S2 glass hybrid samples shows there is a clear difference in behavior between the warp (c) and weft (d) direction. Both of these images suggest that the failure is in fact a microstructure architectural related response.

The failure of the S2 glass is somewhat expected to be nearly identical between the warp and weft direction because of the yarn balance. There are a number of mechanical tests that suggest that the yarn balance is nearly identical, so as expected, the failure modes are quite similar. The kink bands that form in the yarns are very clear. The carbon/S2 glass hybrid shows a much different behavior which could be a result of the microstructure. In the warp direction, it is clear that there are a number of cracks that have formed and some are kink like. In both the upper and lower half of the sample, there are a number of kink bands that have developed. However, there is not a single kink band like that observed in the S2 only glass samples. In the weft direction, it appears as though there is a failure by transverse yarn rupture. This is seen by a number of tows being sheared through, though there still is not a single band of failure. This is due to the addition

of a second z-yarn. This z-yarn arrests the growth of the crack within the layer and acts as an additional energy absorption mechanism.

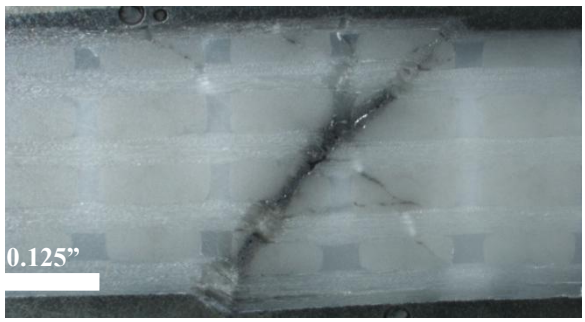

a. S2 glass failure in warp direction.

b. S2 glass failure in weft direction.

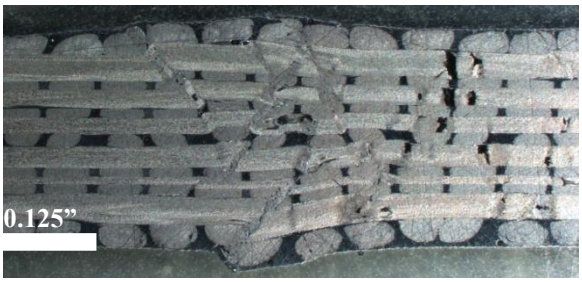

c. Carbon/S2 glass hybrid failure in warp direction.

d. Carbon/S2 glass hybrid failure in weft direction.

Figure 19. Photographs of the failure surfaces for each of the tested surfaces showing that the architecture may affect mechanical performance.

4. Summary and Conclusions

The purpose of this work was to gain a better understanding of how the internal woven architecture of the 3DWC affects the mechanical performance, namely progressive failure and strengths. This work identified how the material behaves under different types of loading.

The first major observation was that the strength and mechanical response of the SC-15 epoxy matrix are different in tension and compression. This is an interesting observation because little work has been done in the past to characterize the difference in mechanical performance in compression versus tension. It was determined that there is an increase in strength about 32% in compression versus tension for samples extracted from the same cured panel. These results are somewhat consistent with literature, although disparities could be contributed to different tests being used to determine mechanical properties such as a flexural test in the case of Zhou et al. (*22*, *23*) and a torsion test in the case of Pankow et al. (*21*).

The woven architecture was vital to the failure of the two types of composites under tensile loading. In both the warp and the weft directions of the S2 glass, matrix pockets created by the z-yarn binding the top weft layers allowed a path for cracks to nucleate and propagate. Progressive failure analysis indicated that when these cracks joined, a large crack across the surface allowed for a fiber tow/matrix interface failure to occur. This was followed by fiber tow pullout, and thusly, a true measure of the tensile strength was not determined. The modulus and failure strengths were approximately the same in this composite, which indicates that the yarn balance in the warp and weft direction is approximately equal.

The carbon/S2 glass hybrid panels displayed less balance in the yarn fractions in the warp and weft direction, as evidenced by the strengths and moduli being much higher in the warp direction versus the weft direction. Analysis of the progression of failure showed that the matrix cracks that developed during loading were arrested by adjacent weft fibers due to the offset z-fiber architecture. This did not allow fiber tow/matrix interface failure that was observed in S2 glass samples and a true tensile failure was observed in the samples.

The S2 glass had a similar response in both the warp and weft direction under compressive loading. The results were generally consistent and micrograph analysis indicated that the mode of failure was via kink band formation. This was observed in both the warp and weft direction. From this we concluded that the architecture has little effect on the compressive strength or mode of failure.

The carbon/S2 glass hybrid panel displayed a more interesting behavior. In particular, there was a difference in the failure types between the warp and weft direction. The weft direction displayed a characteristic shear band/kinking type of failure, whereas the warp had a much more progressive failure in which a number of shear bands develop and appear to be arrested by the two z-yarn architecture. A through thickness shear band does not develop, but rather a series of short bands is observed. This again displays an architectural dependent mechanical behavior.

5. References

1. Olssen, Robin; Donadon, Mauricio V.; Falzon, Brian G. Delamination Threshold Load for Dyanmic Impact on Plates. *International Journal of Solids and Structures* **2006**, *43*, 3124–3141.

2. Experiments. Huang, Hsengji; Waas, Anthony M. Compressive Response of Z-pinned Woven Glass Fiber Textile Composite Laminates. *Composites Science and Technology* **2009**, *69*, 2331–2337.

3. Huang, Hsengji; Waas,, Anthony M. Compressive Response of Z-pinned Woven Glass Fiber Textile Composite Laminates: Modeling and Computations. *Composites Science and Technology* **2009**, *69*, 2338–2344.

4. Mouritz, A. P.; Cox, B. N. A Mechanistic Interpretation of the Comparative In-plane Mechanical Properties of 3D Woven, Stitched and Pinned Composites. *Composites: Part A* **2010**, *41*, 709–728.

5. Dransfield, Kimberley; Baillie, Caroline; Mai, Yiu-Wing. Improving the Delamination Resistance of CFRP by Stitching - A Review. *Composites Science and Technology* **1994**, *50*, 305–317.

6. Tan, K. T.; Watanabe, N.; Iwahori, Y., Ishikawa, T. Effect of Stitch Density and Stitch Thread Thickness on Compression after Impact Strength and Response of Stitched Composites. *Composite Science and Technology* **2012**, *72*, 587–598.

7. Rudov-Clark, S.; Mouritz, A. P.; Lee, L.; Bannister, M. K. Fiber Damage in the Manufacture of Advanced Three-dimensional Woven Composites. *Composites: Part A* **2003**, *34*, 963–970.

8. Lee, L.; Rudov-Clark, S.; Mouritz, A. P.; Bannister, M. K.; Hersberg, I. Effect of Weaving Damage on the Tensile Properties of Three-dimensional Woven Composites. *Composite Structures* **2002**, *57*, 405–413.

9. Cox, Brian N.; Dadkhah, Mahyar S.; Morris, W. L. On Tensile Failure of 3D Woven Composites. *Composites: Part A* **1996**, *27*, 447–458.

10. Cox, B. N.; Dadkhah, M. S.; Morris, W. L.; Flintoff, J. G. Failure Mechanisms of 3D Woven Composites in Tension, Compression, and Bending. *Acta metal. mater.* **1994**, *42*, 3967–3984.

11. Quinn, .P.; McIlhagger, A. T.; McIlhagger, R. Examination of the Failure of 3D Woven Composites. *Composites. Part A* **2008**, *39*, 273–283.

12. Lomov, Stepan V.; Ivanov, Dmitry S.; Verpoest, Ignaas; Zako, Masuro; Kurashiki, Tetsusei; Nakai, Hiroaki; Molimard, Jerome; Vautrin, Alain Full-field Strain Measurements for Validation of Meso-FE Analysis of Textile Composites. *Composites: Part A* **2008**, *39*, 1218–1231.

13. Hale, R. D. An Experimental Investigation into Strain Distributions in 2D and 3D Textile Composites. *Composites Science and Technology* **2003**, *63*, 2171–2185.

14. Ivanov, Dmitry; Ivanov, Sergey; Lomov, Stepan; Verpoest, Ignaas. "Strain Mapping Analysis of Textile Composites. *Optics and Lasers in Engineering* **2009**, *47*, 360–370.

15. ASTM International. ASTM D638: Standard Test Method for Tensile Properties of Plastics. West Conshohocken, PA : ASTM, 2002.

16. Xcitex. ProAnalyst. [Computer Software] 2012.

17. ASTM International. ASTM D695: Standard Test Method for Compressive Properties of Rigid Plastics. West Conshohocken, PA: ASTM, 2008.

18. GOM Optical Measuring Techniques. ARAMIS V6.11. [Computre Software] 2012.

19. ASTM International. ASTM D3039: Standard Test Method for Tensile Properties of Polymer Matix Composite Materials. West Conchohocken, PA: ASTM, 2000.

20. ASTM D6641: Standard Test Method for Compressive Properties of Polymer Matrix Composite Materials Using a Combined Loading Compression (CLC) Test Fixture. West Conchohocken, PA: ASTM, 2009.

21. Pankow, Mark. The Deformation Respose of 3D Woven Composites Subjected to High Rates of Loading. University of Michigan, 2010.

22. Zhou, Yuanxin; Pervin, Farhana; Biswas, Mohammad A.; Rangari, Vijaya K.; Jeelani, Shaik. Frabrication and Characterization of Montmorillonite Clay-filled SC-15 Epoxy. *Materials Letters* **2005**, *60*.

23. Zhou, Yuanxin; Akanda, Sajedur Rahman; Jeelani, Shaik; Lacy, Thoms E. Non-Linear Constitutive Equation for Vapor-grown Carbon Nanofiber-reinforced SC-15 Epoxy at Different Strain Rates. *Material Science and Engineering A* **2007**, *465*, 238–246.

24. Callus, P. J.; Mouritz, A. P.; Bannister, M. K.; Leong, K. H. Tensile Properties and Failure Mechanisms of 3D Woven GRP Composites. *Composites: Part A* **1999**, *90*, 1277–1287.

25. Kuo, W-S; Ko, T-H; Chenc, C-P Effect of Weaving Process on Compressive Behavior of 3D Woven Composites. *Composites: Part A* **2007**, *38*, 555–565.

List of Symbols, Abbreviations, and Acronyms

3DWC	3D Woven Composite
ASTM	American Society for Testing and Materials
CLC	Combined Loading Compression
DIC	Digital Image Correlation
FRPC	Fiber Reinforced Polymer Composite
in	inch
in/min	inch per minute
in/s	inch per second
s	second
TEAM	Textiles Engineering and Manufacturing

NO OF COPIES	ORGANIZATION
1 PDF	1DEFENSE TECH INFO CTR ATTN DTIC OCA (PDF) 8725 JOHN J KINGMAN RD STE 0944 FT BELVOIR VA 22060-6218
3	US ARMY RSRCH LAB ATTN IMAL HRA MAIL & RECORDS MGMT ATTN RDRL CIO LL TECHL LIB ATTN RDRL CIO LT TECHL PUB ADELPHI MD 20783-1197

ABERDEEN PROVING GROUND

1	RDRL WMM B CHIAN-FONG YEN

INTENTIONALLY LEFT BLANK.